

## 5.8 Maximal exchange through a pure contraction with rotation.

One of the fundamental problems of two-layer hydraulics is that of full lock exchange in a channel with a horizontal bottom. We have covered the case of zero background rotation and described the maximal exchange that is set up by the removal of the full depth barrier. If the exchange occurs through a narrows, the flow is critical there and is joined to the end reservoirs by supercritical flows. The solution in the vicinity of the narrows is represented by the curve  $jbk$  of Figure 5.4.1b. In the rotating version of this problem we again imagine a barrier separating fluids of slightly different densities,  $\rho_1$  and  $\rho_2$ , positioned at the narrowest section of a channel that is rectangular in cross section. The channel has constant depth  $D$  and is capped by the usual rigid lid. When the barrier is removed the two fluids begin to move in opposite directions, thrusting under and over each other as before. With northern hemisphere rotation, each layer veers to its right as it intrudes. The potential depth  $D_{n\infty}$  of layer  $n$  is its initial depth  $D$ , whereas the average depth of each layer after at the narrows after adjustment  $D/2$ . The severe vortex squashing that is inherent in rotating flow over a shallow flow is therefore lacking and use of the zero potential vorticity approximation, which depends on this process, is no longer valid. The nondimensional potential vorticity, while uniform in each layer, must now be considered non-zero. Although one anticipates that the final state, be it steady, will have maximal exchange, this is not formally shown.

Historically, two approaches have been used to predict the steady flow state that results from the lock exchange problem without rotation. In the first, one simply assumes that the flow at the original position of the dam becomes hydraulically critical ( $G^2=1$ ). This along with the symmetry properties of the full lock exchange are sufficient to find the final steady state, namely the aforementioned hydraulic solution. The second approach is based on an energy balance for the evolving solution (Yih, 1980). The calculation is straightforward when the channel is considered uniform in  $y^*$ , and perhaps linked to reservoirs far upstream and downstream of the initial barrier. Destruction of the barrier results in the formation of the intrusions suggested in Figure 5.8.1a. An idealization of the lower intrusion is that it consists of a nose region, followed by a steady flow with uniform depth  $D/2$  and uniform velocity  $v^*$ . The upper layer intrusion has the same depth but equal and opposite velocity. The energy argument attempts to calculate  $v^*$ , and thereby the layer fluxes, by equating the potential energy lost to kinetic energy gained as a result of the adjustment. The procedure is unable to account for dissipation that might occur in the nose regions, or for the detailed structure those regions.

At the time frame shown in Figure 5.8.1a, the steady portions of the intrusions occupy a distance  $L$ . The two-layer density distribution in this region (Frame c) can be created from the initial distribution (Frame b) by interchanging regions I and II. Doing so lifts each parcel in II a distance  $D/2$ , thereby increasing its potential energy by amount  $g\rho_1 D/2$ . The volume of region II is  $w^*(D/2)(L/2)$  and thus the total increase in potential energy is  $g\rho_1 D^2 L /8$ . Similarly, region I sees a  $D/2$  drop in elevation, and a total decrease in potential energy equal to  $g\rho_2 D^2 L /8$ . The net decrease in potential energy is therefore

$g(\rho_2 - \rho_1)D^2Lw^*/8$ . The kinetic energy gained in the same volume is clearly  $(\rho_1v^{*2} + \rho_2v^{*2})DLw^*/4$ . Equating the potential energy lost to the kinetic energy gained leads to

$$v^* = \sqrt{\frac{gD(\rho_2 - \rho_1)}{2(\rho_1 + \rho_2)}}, \quad (5.8.1)$$

which is equivalent to  $G^2=1$ . Thus the energy balance and the hypothesis of critical flow lead to the same result.

If the fluid is rotating, a similar energy balance can be invoked, but now the cross-stream variation of speed and depth must be included. The following generalizes a calculation due to Hunkins and Whitehead (1992). It is again assumed that the channel is uniform, the adjusted flow is steady and that there is no energy loss. As we will see later, the assumption of steadiness becomes questionable when the channel width exceeds the internal radius of deformation  $L_I$ , as given by (5.1.12). The latter is simplified by  $D=D_{1\infty}=D_{2\infty}$ , leading to  $L_I = \sqrt{g'D/2f^2}$ . Since the upper and lower layer should behave as mirror images, the interface height will be antisymmetric with respect to  $x^*$ . The solutions to (5.1.11) with this property are

$$d_1^* = \frac{D}{2} - A \sinh \frac{x^*}{L_I}, \quad (5.8.2)$$

and

$$d_2^* = \frac{D}{2} + A \sinh \frac{x^*}{L_I}. \quad (5.8.3)$$

The corresponding along-channel velocities are determined by (5.1.8) and (5.1.9) as

$$v_1^* = V^* - \frac{fx^*}{2} - \frac{fL_I}{D} A \cosh \frac{x^*}{L_I} \quad (5.8.4)$$

$$v_2^* = V^* - \frac{fx^*}{2} + \frac{fL_I}{D} A \cosh \frac{x^*}{L_I}, \quad (5.8.5),$$

where  $V$  is a constant. The net (barotropic) flux  $Q_b = \int_{-w^*/2}^{w^*/2} (v_1^* d_1^* + v_2^* d_2^*) dx$  can be shown to be equal to  $V^*Dw^*$  and thus  $V^*=0$  for zero net exchange.

It remains only to determine the coefficient  $A$  in terms of the channel width  $w^*/L_I$ . Following the previous argument, the loss of potential energy is equated with the gain in kinetic energy of the hypothetical steady state. The calculation is a bit more involved

because both the layer depths and velocities vary across the channel. The interested reader may wish to work through Exercise 1 to see the details and to verify the result:

$$g' \int_{-w^*/2}^{w^*/2} \left( \frac{D^2}{2} - d_2^{2*} \right) dx^* = \frac{1}{4} \int_{-w^*/2}^{w^*/2} \left( v_2^{2*} d_2^* + v_1^{2*} d_1^* \right) dx^* \quad (5.8.6)$$

Use of (5.8.2-5) then yields

$$\frac{w_s^{3*}}{24L_I^3} + \frac{A^2}{D^2} \left[ \frac{w^*}{L_I} \left( 1 - \cosh \frac{w^*}{L_I} \right) + 4 \sinh \frac{w^*}{L_I} \right] = \frac{w^*}{L_I} \left( 1 + \frac{2A^2}{D^2} \right) \quad (5.8.7)$$

The volume flux of each layer is given by

$$Q_1^* = -Q_2^* = \int_{-w^*/2}^{w^*/2} d_1^* v_1^* dx^* = fAL_I \left( \frac{w^*}{2} \cosh \frac{w^*}{2L_I} - 2L_I \sinh \frac{w^*}{2L_I} \right). \quad (5.8.8)$$

The layer fluxes can be calculated as a function of  $w^*/L_I$  by eliminating  $A$  between this equation and (5.8.7). The resulting relation is shown as a dashed curve in Figure 5.8.2. It is not difficult to verify that the limiting case of zero rotation (5.8.1) is approached for  $w^*/L_I \rightarrow 0$ . For comparison, the flux predicted by zero potential vorticity theory (Eq. 5.7.22) is shown as a dotted curve.

The foregoing analysis is valid as long as the interface stays in contact with both channel walls. Separation first occurs when  $d_1^*(w^*/2) = d_2^*(-w^*/2) = 0$ , which corresponds to  $w^* = w_s^*$ , where

$$A \sinh \frac{w_s^*}{2L_I} = \frac{D}{2},$$

in view of (5.8.2). If this expression is then used to eliminate  $A$  from (5.8.6), one obtains  $w_s^*/L_I = 1.459$  and  $A/D = 0.628$  (correcting a numerical mistake in Hunkins and Whitehead, 1992). The corresponding value of  $Q_2^*$  is given by  $.208gD^2/f$ .

As an alternative to the energy argument, one might invoke a critical condition for the adjusted flow. The latter has been derived for the case of the flow in question by Rabe et al. (2006) as

$$A^2 \frac{8L_I}{w^*} \cosh^2 \frac{w^*}{2L_I} \sinh \frac{w^*}{2L_I} - 2 \cosh \frac{w^*}{2L_I} + \frac{w^*}{2L_I} \sinh \frac{w^*}{2L_I} = 0 \quad (5.8.9)$$

The mechanics of this calculation are discussed in Exercise 3. The flux is obtained by eliminating  $A$  between (5.8.8) and (5.8.9) and is shown by the solid curve in Figure 5.8.2.

The limiting separation width and flux are given by  $w^*/L_I=1.63$  and  $Q_2^*=0.176g'D^2/f$ . Note that, unlike the case of zero rotation, these results differ from what is predicted by the energy argument.

For  $w^*>w_s^*$  the flow becomes separated from both walls resulting in central, baroclinic region ( $-w_s^*/2<x^*<w_s^*/2$ ) occupied by both layers and flange regions occupied by only layer (Figure 5.8.1e). In the case of zero potential vorticity, the flange regions contain horizontal shear equal to  $-f$ . In the present setting, where the flange region depth  $D$  is also the potential depth of the occupying layer, the shear is zero. If the velocity remains continuous throughout each layer, the uniform velocity  $v_n^*$  in a flange region must equal the velocity at the edge of the barotropic region. For example, the value of  $v_2^*$  in the right-hand flange  $w_s^*/2<x^*<w^*/2$  must equal its value at  $x^*=w_s^*/2$ . The corresponding flow must be included in the total flux for layer 2 and this added flux increases in proportion to the channel width  $w^*$ . An alternative idea, proposed by Whitehead et al. (1974) and also used by Hunkins and Whitehead (1992), is that the flange regions are motionless. In this case the layer velocities are discontinuous at the edges of the central region. The layer fluxes then become independent of  $w^*$  and are just those given by the above theories in the limiting case  $w^*=w_s^*$ . These values are summarized by

$$\frac{Q_2^* f}{g'D^2} = \begin{array}{l} 0.208 \quad (w^*/L_I > 1.46.. \text{ WH92}) \\ 0.176 \quad (w^*/L_I > 1.63... \text{ Rabe et al.06}) \\ 1/6 \quad (w^*/L_I > \sqrt{2}, \text{ WLK74}) \end{array} \quad (5.8.10)$$

The  $w^*$ -independent flux values given by (5.8.10) are indicated by the horizontal lines that extend the three curves in Figure 5.8.2. These lines give the hypothetical flux determined by the respective theory for  $w^*>w_s^*$ , assuming that the flange regions are quiescent.

Rotating lock exchange flow has been simulated in a number of laboratory experiments, including Whitehead et al. (1974), Dalziel (1988), and Hunkins and Whitehead (1992). In addition Rabe et al. (2006) carried out both laboratory and numerical simulations. Some of the experiments make use of a uniform length of channel, assumed in the energy argument, that separate two broad reservoirs. In other cases the reservoirs are separated by a smoothly varying channel that has a minimum width at a single section. Photographs from the Hunkins and Whitehead experiment show four realizations of the experiment for different Rossby radii (Figure 5.8.3), all in the range of predicted separation. Each pair of images shows the same parameter values: in the first frame the (leftward moving) fresh layer is dyed and in the second the (rightward moving) salt water is dyed. Eddies and filaments are evident on the interface between the two fluids in all cases and not exhibit complete separation from both sidewalls. The value of  $Q_1^*$  ( $=Q^*$ ) can be measured indirectly by replacing the barrier after a set time, mixing the two fluids within each reservoir, and calculating the density change between the two mixed reservoirs. In the case of Rabe et al. (2006) direct velocity measurements based on digitally imaged drifting particles were also used to estimate the flux.

The fluxes measured in all the experiments show increased scatter (as do the predictions) as the channel width is increased relative to  $L_I$  (Figure 5.8.2). The three theories are quite close, and do a good job of predicting the flux, when  $w^*/L_I$  is small. The experimental are generally overestimated by predictions. The most problematic region over which to compare theory and observation is that where flow separation is predicted, roughly  $f w^*/(g'D/2)^{1/2} > 1.5$  in Figure 5.8.2. Although double separation of the flow is predicted, it is not observed in any of the experiments. In some cases, separation of just one layer is observed, in others the picture is clouded by the presence of eddies. The predictions for  $Q_2^* f/g'D^2$  are given by the horizontal lines, and these capture the weak dependence on the dimensionless channel width that is observed. Improvement in the prediction of the fluxes themselves in this regime will require a better understanding of the flow itself.

We also note that  $1/6$  coefficient in equation (5.8.9) has been used as an estimate for flux rate in applications to Spencer Gulf, South Australia, (Bye and Whitehead 1975) and Chesapeake Bay, North America (Whitehead, 1989b). Hunkins and Whitehead (1982) used (5.8.14a) to estimate an exchange of freshwater for the Arctic Ocean, and found that the exchange was consistent with an observed salinity difference of about 1 psu between outflowing water and inflowing water at Fram Strait. The agreement was necessarily very crude because of the many other important features such as the great width and depth of Fram Strait, wind driven currents, and rafted sea-ice.

## Exercises

1. *Energy balance for a rotating lock exchange.* Consider the hypothetical adjusted state that results from lock exchange in a rotating channel. The steady exchange flow has a cross-section suggested in Figure 5.8.1d and the flow itself extends over a distance  $L$ , as in frame a.

(a) Show that the levels of centers of mass,  $\bar{z}_1$  and  $\bar{z}_2$ , of the two moving layers are given by

$$\bar{z}_2 = \frac{2}{wD} \int_{-w/2}^{w/2} \frac{1}{2} d_2^2 dx \quad \bar{z}_1 = \frac{2}{wD} \int_{-w/2}^{w/2} \frac{1}{2} (D^2 - d_2^2) dx$$

(b) Argue, perhaps using a sketch, that that loss of potential energy of the flow within the length  $L$  is given by

$$\frac{1}{2} g(\rho_2 - \rho_1) L w^* (\bar{z}_1 - \bar{z}_2)$$

(c) Equate this loss with the gain in kinetic energy:

$$\frac{1}{2}L \int_{-w^*/2}^{w^*/2} (\rho_1 d_1^* v_1^{*2} + \rho_2 d_2^* v_2^{*2}) dx^*$$

and thereby verify, after use of the Boussinesq approximation, Equation (5.8.6).

2. Show that using (5.8.7) in (5.8.8) produces a formula that approaches equation (5.8.1) as rotation becomes small.

3. *Derivation of critical condition for two-layer flow with both potential depths equal to D:* Consider an attached, two-layer flow with  $D=D_{1\infty}=D_{2\infty}$ , as occurs in the lock exchange.

(a) By referencing the appropriate relations in Section 5.1, show that the velocity and depth profiles are given by

$$d_1^* = \frac{D}{2} - A \sinh \frac{x^*}{L_l} - C \cosh \frac{x^*}{L_l}, \quad (5.8.12)$$

$$d_2^* = \frac{D}{2} + A \sinh \frac{x^*}{L_l} + C \cosh \frac{x^*}{L_l}, \quad (5.8.13)$$

$$v_1^* = V^* - \frac{fx^*}{2} - \frac{fL_l}{D} \left[ A \cosh \frac{x^*}{L_l} + C \sinh \frac{x^*}{L_l} \right], \quad (5.8.14)$$

and

$$v_2^* = V^* - \frac{fx^*}{2} + \frac{fL_l}{D} \left[ A \cosh \frac{x^*}{L_l} + C \sinh \frac{x^*}{L_l} \right]. \quad (5.8.15)$$

(b) Show using these expressions that the layer fluxes are given by

$$Q_1^* = \frac{1}{2}DV^*w^* + \frac{1}{2}AfL_lw^* \cosh \left[ \frac{w^*}{2L_l} \right] - 2L_l(AfL_l + CV^*) \sinh \left[ \frac{w^*}{2L_l} \right] + (ACfL_l^2 / D) \sinh \left[ \frac{w^*}{L_l} \right]$$

and

$$Q_2^* = \frac{1}{2}DV^*w^* - \frac{1}{2}AfL_lw^* \cosh \left[ \frac{w^*}{2L_l} \right] + 2L_l(AfL_l + CV^*) \sinh \left[ \frac{w^*}{2L_l} \right] + (ACfL_l^2 / D) \sinh \left[ \frac{w^*}{L_l} \right], \quad (5.8.16)$$

and therefore that the net (barotropic) flux is given by

$$Q_b^* = Q_1^* + Q_2^* = DV^* w^* + (2CAfL_d^2 / D) \sinh\left[\frac{w^*}{L_d}\right]. \quad (5.8.17)$$

b. Evaluate the internal Bernoulli function along the right wall and show that

$$\Delta B^*_{x^*=w^*/2} = \frac{fL_d}{2D} \left\{ \begin{aligned} &2DfL_d + (4CfL_d + 4AV^* - Afw^*) \cosh\left(\frac{w^*}{2L_d}\right) \\ &+ (4AfL_d + 4CV^* - Cfw^*) \sinh\left(\frac{w^*}{2L_d}\right) \end{aligned} \right\} \quad (5.8.18)$$

c. Note that (5.8.16-18) define three hydraulic functions in the three variables  $A$ ,  $C$ , and  $V^*$ . Apply (1.5.14) to these functions to obtain the critical condition

$$\begin{aligned} &f^2 L_d w^* \left[ (C^2 + A^2) L_d \sinh\left(\frac{w^*}{L_d}\right) - D^2 w^* \right] \cosh\left(\frac{w^*}{L_d}\right) \\ &= \left[ w^* \left( (A^2 - C^2) f^2 L_d^2 + D^2 (f^2 (2L_d^2 + w^{*2} / 8) - 2V^{*2}) \right) \right. \\ &\quad \left. - 4fL_d^2 \left( (C^2 + A^2) fL_d - 2CAV^* \right) \sinh\left(\frac{w^*}{L_d}\right) \right] \sinh\left(\frac{w^*}{L_d}\right) \end{aligned} \quad (5.8.19)$$

(Note that a symbolic manipulation program will be helpful in doing the bookkeeping.)

d. For conditions of zero net flux, and an asymmetrical interface (w.r.t.  $x^*$ ), show that (5.8.19) reduces to the desired condition (5.8.9).

## Figure Captions

Figure 5.8.1. a: The gravitational advance of two mutual intrusions of differing density in a channel. b and c: Side views of the initial density distribution and an idealization of the adjusted density. d and e: Schematic cross-section for the adjusted flow in the lock exchange with rotation.

Figure 5.8.2. The dimensionless volume flux vs. dimensionless channel width. The three curves give predictions based on the theories of Whitehead et al. 1974 (dotted); Hunkins and Whitehead 1992 (dashed); and Rabe et al. 2006 (solid). The first two of these have been extended as horizontal lines to indicate the width-independent flux hypothesized by the authors for the case in which the flow detaches from the sidewalls. The data points corresponds to laboratory experiments by Hunkins and Whitehead 1992 (small dots);

Dalziel 1988 (circles); and Rabe et al. 2006 (triangles). Note the factor  $2^{1/2}$  change in the scale for  $w^*$  relative to Section 2.7.

Figure 5.8.3. Top view of dye spreading after approximately 60 seconds. Starting from the top, the photographs show successively the layer of dyed freshwater (originating on the right) and then dyed saltwater (originating on the left). Each pair downwards has more rapid rotation, with  $w^*f/(g'D)^{1/2}=1.2, 2.5, 5.0$  and  $10.0$ , respectively. Based on the experiments of Hunkins and Whitehead (1992).

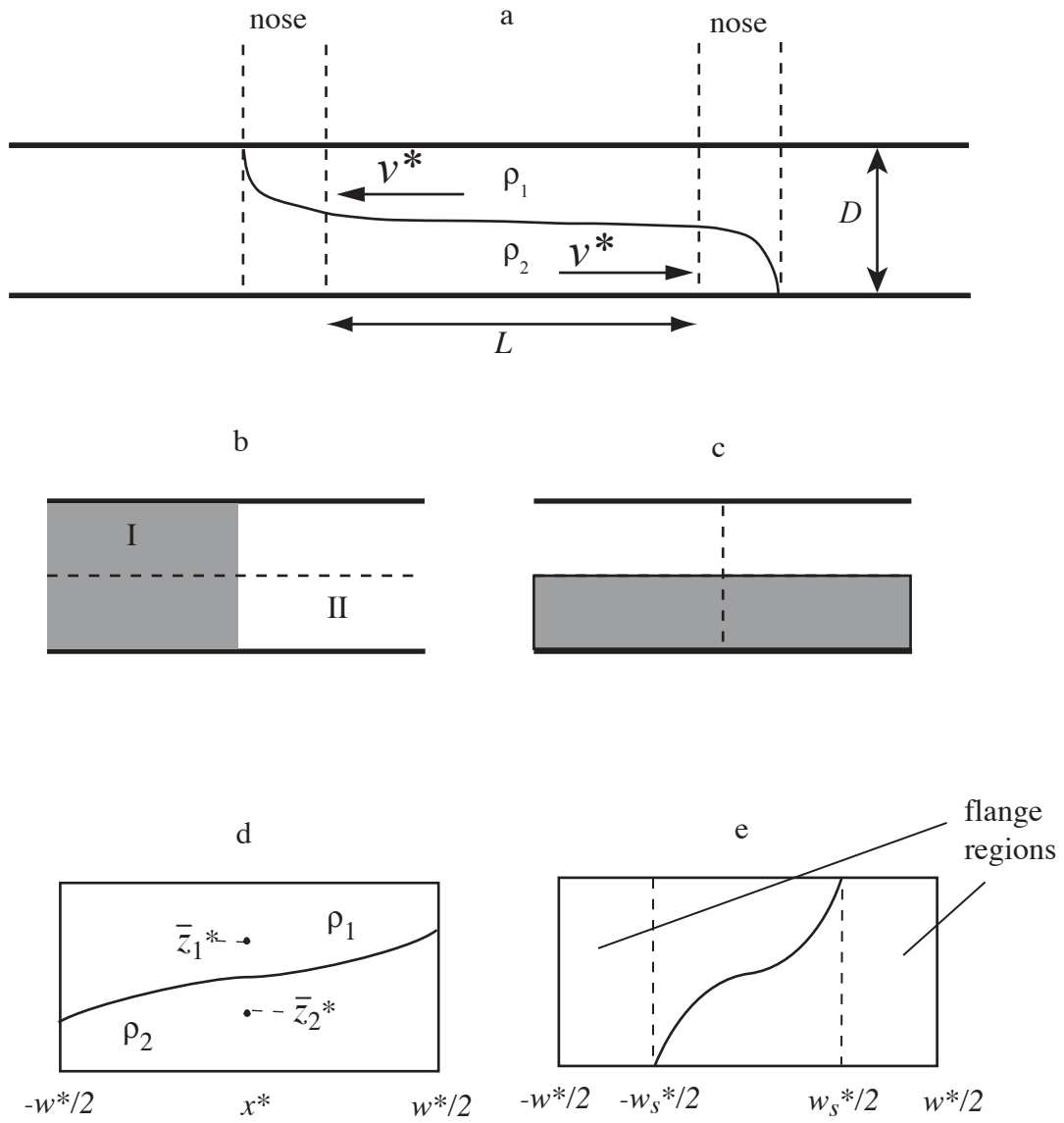


Figure 5.8.1

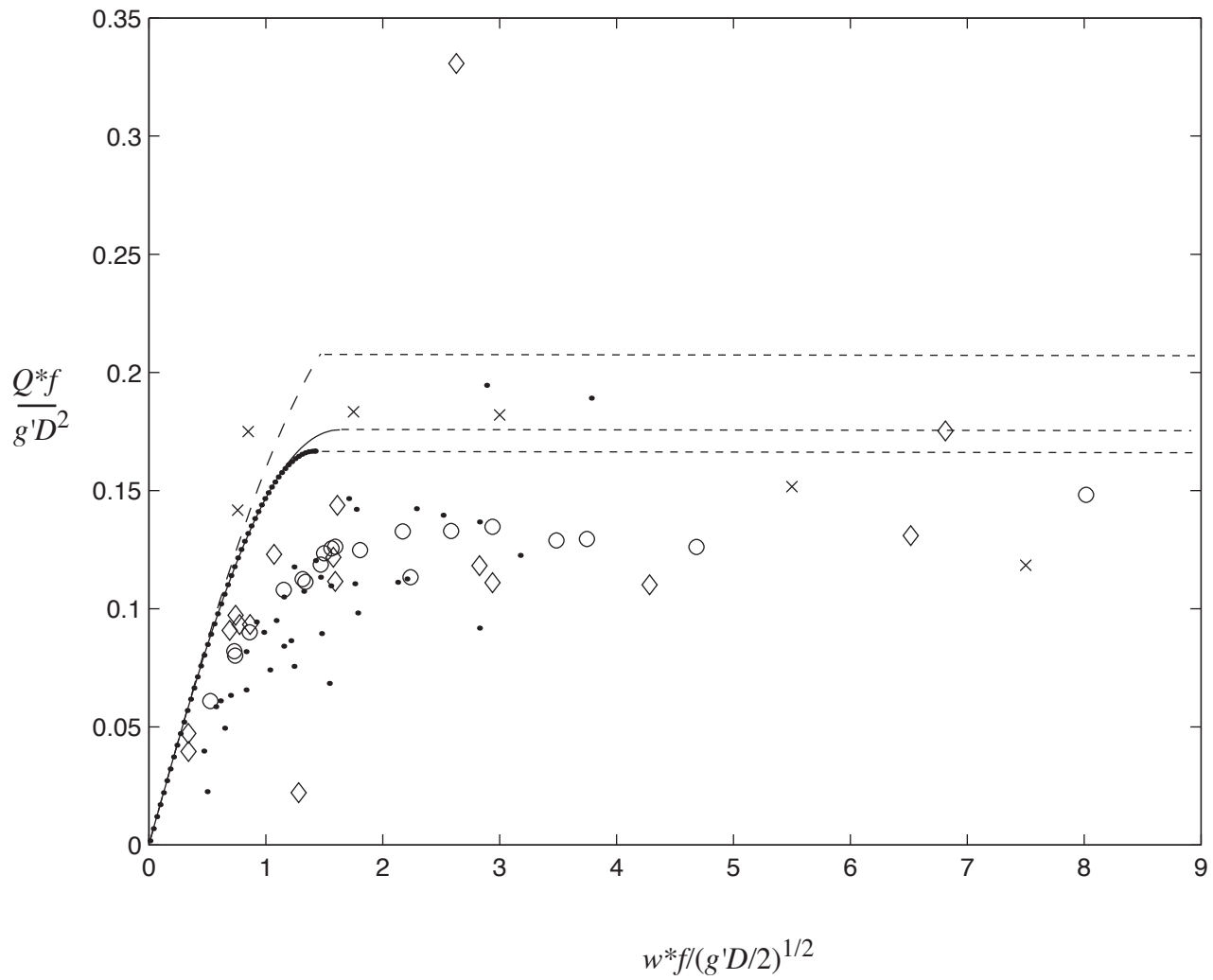


Figure 5.8.2

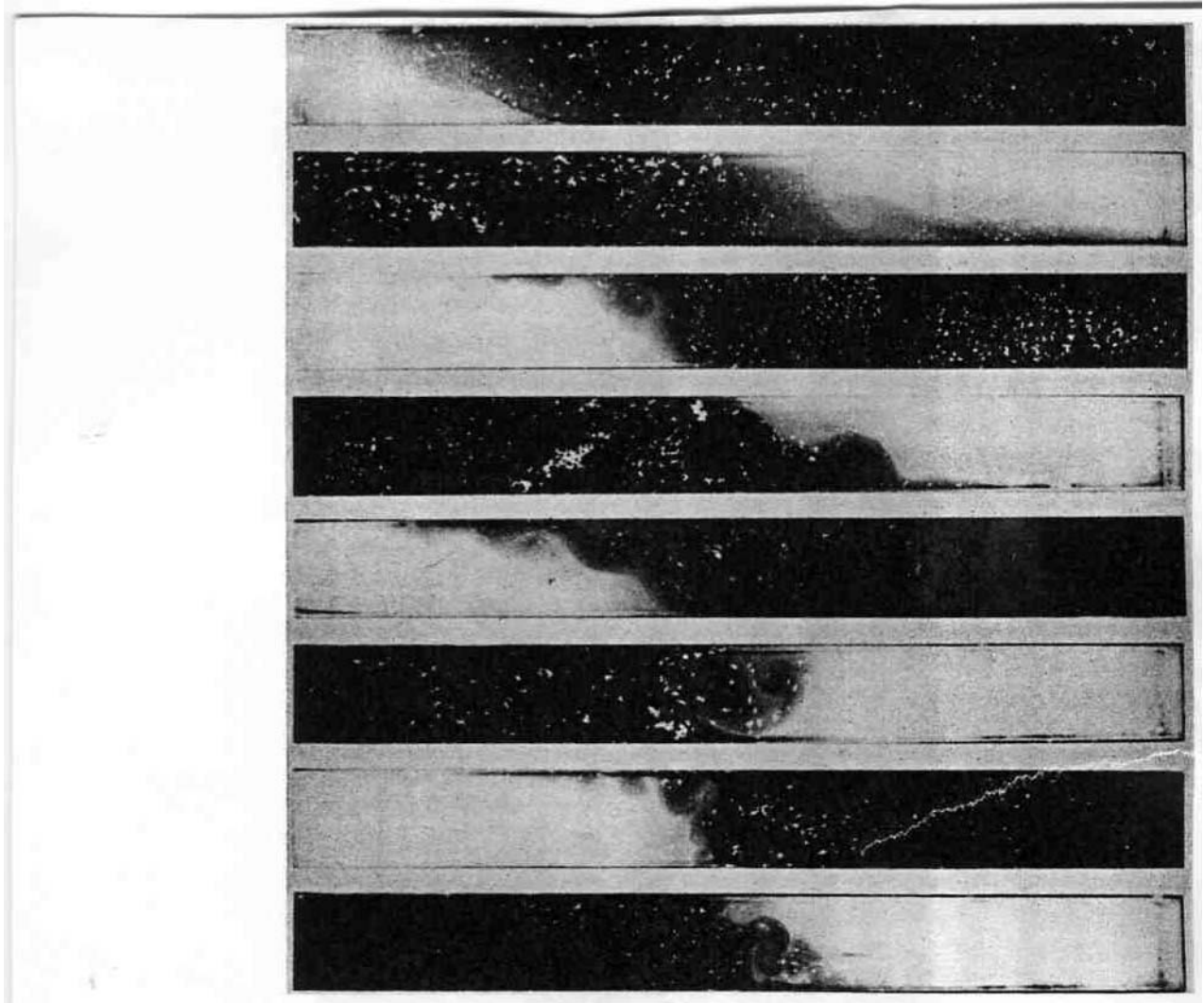


Figure 5.8.3 low resolution version